Engineering Solid Mechanics 9 (2021) 363-376

Contents lists available at GrowingScience

Engineering Solid Mechanics

homepage: www.GrowingScience.com/esm

Stress intensity factor computation of inclined cracked tension plate using XFEM

Migbar Assefa Zeleke[a,b*], Edward Dintwa[a] and Kevin N. Nwaigwe[a]

[a]*Department of Mechanical Engineering, University of Botswana, Botswana*
[b]*Department of Mechanical Engineering, Hawassa University, Institute of Technology, Ethiopia*

ARTICLE INFO

Article history:
Received 12 May 2021
Accepted 16 July 2021
Available online
16 July 2021

Keywords:
Inclined Cracked tension plate
Mixed mode I/II
Stress intensity factors (SIFs)
XFEM

ABSTRACT

One of the major successes in the field of Linear Elastic Fracture Mechanics (LEFM) is the groundwork of the stress intensity factor (SIF) computation. The approaches used to carry out SIF values may be analytical, semi-analytical, experimental or numerical. Each one of the above methods has its own benefits however the use of numerical solutions has become the most frequent and popular. Numerous schemes for the numerical computation of SIF have been developed, the J-integral method being the most popular one. In this article we examine the SIFs of an edge cracked two dimensional (2-D) steel plate subjected to tensile loading. Extended finite element (XFEM) computational scheme has been employed to estimate the values of SIF. The SIF values of cracks with different lengths and inclination angles (different configurations) have been examined by utilizing the domain based interaction integral approach. The effect of crack inclination and crack position on SIFs (K_I and K_{II}) has also been studied. The results obtained in this study were compared with those from literature and theoretical values and observed that they are in close agreement.

1. Introduction

Fracture is one of the most challenging failure modes in engineering and resulted from material instability in mechanical or structural components normal to the discontinuity (Belytschko et al., 2014). In many engineering fields, several terrible accidents are mainly originated from defects like micro-cracks and voids. Thus, research developments in the area of fracture mechanics are crucial. One of the key achievements in the field of Linear Elastic Fracture Mechanics (LEFM) is the concept of the stress intensity factor (SIF). The basic and fundamental stress intensity factor was introduced by Irwin (1957) and he investigated that SIF is a crucial parameter that uniquely describes the stress field in the neighborhood of crack tip. Additionally, SIF provides information about the direction and speed of moving crack, hence its determination is quite convenient to decide crack growth rate (Paris & Erdogan, 1963). In general, SIF is a function of crack size, crack location, geometry of specimen and magnitude and distribution of load intensity (Pais, 2011). Currently there are numerous techniques in the calculation of SIF, but the energy release approach and the field variable approach are the most frequently adopted numerical approaches to extract SIFs (Murakami & Keer, 1993; Lins et al. 2015). The energy release approach includes the J-integral (Rice, 1968) the stiffness derivative method (Parks, 1974) the Interaction

* Corresponding author.
E-mail addresses: zelekem@ub.ac.bw (M. A. Zeleke)

doi: 10.5267/j.esm.2021.7.002

Integral Method (Moran & Shih, 1987) the virtual crack extension method (Hellen, 1975) the Contour Integral Method (Stern et al., 1976; Szabo & Babuška, 1988) and the virtual crack closure technique as developed by (Rybicki & Kanninen, 1977). The field variable approaches on the other hand can be segmented into stress based techniques and displacement based techniques. The displacement based technique encompasses the quarter-point displacement method (Barsoum, 1974; Henshell and Shaw, 1975) and the displacement correction method (Shih et al., 1976). Based on the principles of LEFM, Finite Element Method (FEM) (Han et al., 2015; Fayed, 2017; Leung et al., 2014; Bhadauria et al., 2010; El Fakkoussi et al., 2019) and Boundary Element Method (BEM) (Gonzalez et al., 2015; Ortiz & Cisilino, 2006; Portela et al., 1992) have been widely employed for years to determine SIFs.

It is well known that flaws like scratches, micro-cracks or other forms of discontinuities are inevitable during the fabrication of mechanical components. These discontinuities considerably affect the performance of a component by creating theoretically infinite stresses near the crack tip. The presence of discontinuities also creates interruption of operation, failure or even terrible accidents. Therefore, it is vital to give attention to the design and analysis of mechanical components with flaws. One of the most versatile and flexible numerical tools that solve a variety of engineering problems in the history of computational mechanics is the finite element method (FEM). While FEM is an effective and well established method of solving engineering problems, it has got its own constraints in the modeling and analysis of fracture problems (Belytschko & Black, 1999). One major constraint of the method is its dependency on mesh density. To capture the field variables near the crack tip FEM requires a fine and conformal mesh. Furthermore in the case of moving cracks FEM demands remeshing whenever the crack moves. To bypass the above restrictions faced by standard FEM, researchers proposed both meshless and mesh based (Belytschko et al., 1994; Belytschko et al., 1994; Lu et al., 1994; Liu et al., 1995; Rabczuk & Belytschko, 2004; Ching & Yen, 2005; Gu et al., 2011; Lee et al., 2016) numerical schemes. (Moes et al., 1999) pushed forward the standard FEM by adding an enrichment function with additional degrees of freedom at the crack surfaces and crack tip. For the last two decades researchers have significantly studied XFEM as a solution tool in area of engineering and science due to its versatility in simplifying problems with discontinuities (Belytschko & Black, 1999; Moes et al., 1999; Menk & Bordas, 2011; Singh et al., 2012; Bouhala et al., 2013; Ameri et al., 2021; Mirmohammad et al., 2018, Aliha et al., 2016;2020,2021). In XFEM the standard FEM equations are supplemented with additional functions called enrichment functions. SIF computation of a slanted central crack of aluminum plate using ABAQUS XFEM package has been demonstrated in (Hedayati & Vahedi, 2014). In this article the authors estimated the life of the structure using ABAQUS XFEM tool. Similarly (Laftah, 2016) used the general finite element software ABAQUS to study the influence of crack length on the determination of SIF of corrugated plate. Therefore, the aim of this article is to develop XFEM formulation to compute the stress intensity factor of 2-D steel plates with edge cracks at different locations and angular positions. In this study, the effect of crack orientation angles and positions on the SIFs will also be considered. Mode I/II SIFs at different crack locations along the height of the plate were studied. In this article the domain based interaction integral scheme has been implemented on MATLAB to compute the SIFs. To the best of the authors' knowledge no one studied the SIF determination of slant cracked steel plate using XFEM by taking into account the indicated parameters.

2. Properties and Model Geometry of Plate

For demonstration purpose a plate having an edge crack with different inclination angles β subjected to tensile loading has been considered as shown in Fig. 1. Inclined crack geometry and its boundary conditions are also illustrated in Fig. 1. The bottom edge of the plate is constrained in the y direction and the top edge is subjected to uniform tensile stress of $\sigma_0 = 10$ MPa. The following dimensions and material properties are considered. The dimensions and material properties of the plate for this study are adopted from (Fayed, 2017) where the height of the plate (*2D*) is 20 cm, and its width (*L*) is 10 cm. Furthermore, the elastic modulus (E) and Poisson's ratio (ν) are 206 GPa and 0.3, respectively. In this study, crack length to width ratios (*a/L*) of 0.1, 0.2, 0.3, 0.4, and 0.5 has been considered with that of variations in the crack angle β between 0° and 75°. The crack angle β measured counterclockwise with reference to the horizontal axis. The other parameter considered in this study was the relative crack positions along the height (*d/D*) ranging from 0 to 0.7 with 0.1 increments were analyzed.

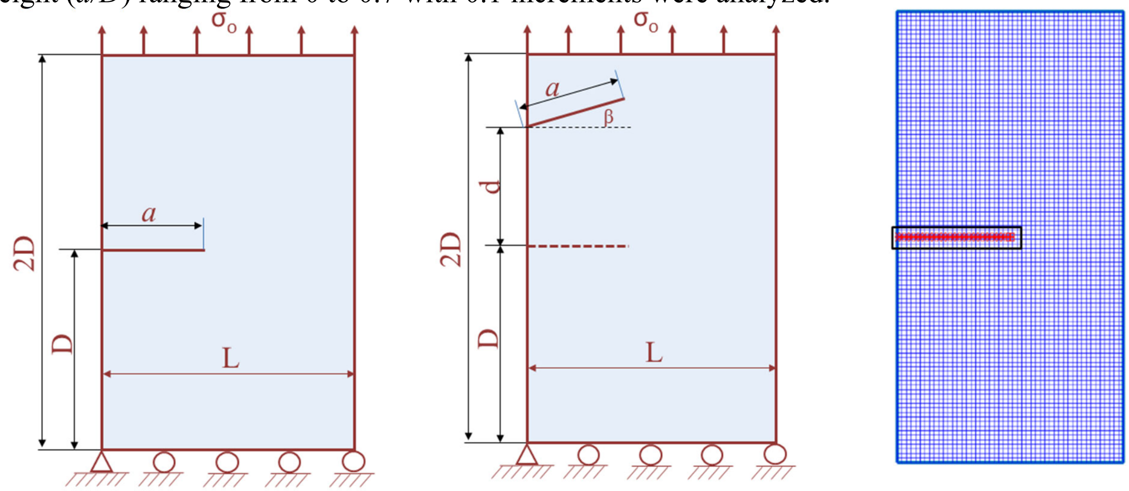

a) Edge crack b) Inclined crack c) discretization

Fig. 1. Dimensions and boundary conditions of an edge cracked tension plate.

3. Numerical implementation and Governing Equation

Consider a body with domain Ω which is bounded by (Γ). The boundary (Γ) comprises displacement (Γ_u), traction free (Γ_c) and traction (Γ_t) boundary conditions as depicted in Fig. 2. According to (Pommier et al., 2011) the equilibrium equations are expressed as:

$$\nabla \cdot \boldsymbol{\sigma} + \mathbf{b} = 0 \quad \text{in } \Omega \tag{1}$$

$$\boldsymbol{\sigma} \cdot \mathbf{n} = \bar{\mathbf{t}} \quad \text{on } \Gamma_t \tag{2}$$

$$\boldsymbol{\sigma} \cdot \mathbf{n} = 0 \quad \text{on } \Gamma_c \tag{3}$$

where, $\boldsymbol{\sigma}$, $\mathbf{b}$, $\nabla \cdot$ and $\mathbf{n}$ represent stress tensor, body force per unit volume divergence operator and outward normal respectively. The following kinematic equations may be applied for small displacements:

$$\boldsymbol{\varepsilon} = \boldsymbol{\varepsilon}(\mathbf{u}) = \nabla_s \mathbf{u} \tag{4}$$

Its boundary condition is

$$\mathbf{u} = \bar{\mathbf{u}} \quad \text{on } \Gamma_u \tag{5}$$

where, $\boldsymbol{\varepsilon}, \mathbf{u}$ and ∇_s denote strain, displacement vector and the symmetric portion of gradient operator respectively.

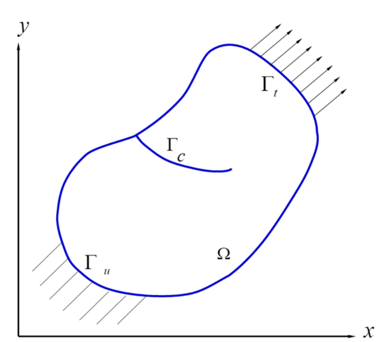

Fig. 2. Domain with crack and different boundary conditions.

For linearly elastic materials the constitutive relation is given as:

$$\boldsymbol{\sigma} = \mathbf{D}\boldsymbol{\varepsilon} \tag{6}$$

where $\boldsymbol{\varepsilon}$ is the strain and $\mathbf{D}$ is Hook's tensor and it is given as follows:

$$\mathbf{D} = \frac{E}{(1+\nu)(1-2\nu)}\begin{bmatrix} 1-\nu & \nu & 0 \\ \nu & 1-\nu & 0 \\ 0 & 0 & \frac{1-2\nu}{2} \end{bmatrix} \quad \text{plane strain} \tag{7}$$

$$\mathbf{D} = \frac{E}{1-\nu^2}\begin{bmatrix} 1 & \nu & 0 \\ \nu & 1 & 0 \\ 0 & 0 & \frac{1-\nu}{2} \end{bmatrix} \quad \text{plane stress} \tag{8}$$

In Eq. (7) and Eq. (8) ν and E represent Poisson's ratio and Young's modulus respectively. The weak form of governing equilibrium equation can be written as:

$$\int_{\Omega} \boldsymbol{\sigma}(\mathbf{u}) : \boldsymbol{\varepsilon}(\mathbf{v})\, d\Omega = \int_{\Omega} \mathbf{b}.\mathbf{v}\, d\Omega + \int_{\Gamma_t} \bar{\mathbf{t}}.\mathbf{v}\, d\Gamma \tag{9}$$

Fig. 3 shows the graphical representation of split elements that are enriched with Heaviside function (red circles) and tip elements enriched with complex functions (blue squares).

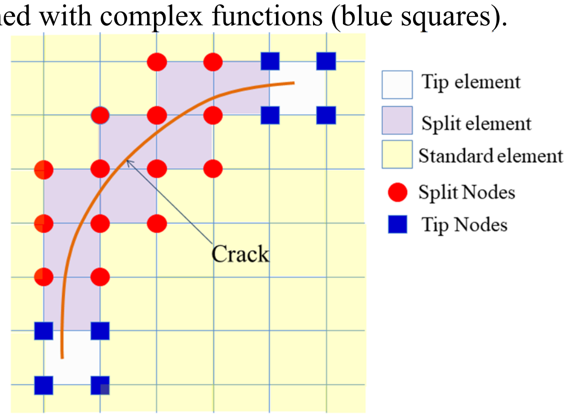

Fig. 3. Nodes enriched with Heaviside and crack tip functions.

3.1 Edge Crack Modeling using XFEM

The XFEM mesh does not require conforming to the geometry of the crack unlike standard FEM where remeshing is mandatory and hence XFEM is quite efficient in modeling discontinuities. According to (Sukumar et al., 2001; Moes et al., 1999) displacement function for 2-D crack modeling is approximated as:

$$\mathbf{u}^{\mathrm{h}}(\mathbf{x}) = \sum_{j=1}^{n} \Psi_j(\mathbf{x}) \left[\bar{\mathbf{u}}_j + \underbrace{\left[H(\mathbf{x}) - H(\mathbf{x}_{\mathrm{i}})\right]\mathbf{a}_j}_{j\varepsilon n_s} + \underbrace{\sum_{\alpha=1}^{4}\left[\beta_\alpha(\mathbf{x}) - \beta_\alpha(\mathbf{x}_{\mathrm{i}})\right]\mathbf{b}_j^{\alpha}}_{j\varepsilon n_t} \right], \tag{10}$$

where $\bar{\mathbf{u}}_j$ is a vector related to standard FEM degrees of freedom (DOF). n represents the entire nodes of the mesh, n_s stands for those node sets entirely crossed by the crack, n_t signifies node sets belong to elements partly cut by the crack. $\mathbf{a}_j$ represents the nodal DOF supplementing Heaviside function and $\mathbf{b}_j^{\alpha}$ represents the nodal DOF supplementing tip enrichment, $\beta_{\alpha}(\mathbf{x})$.

The tip enrichment function $(\beta_{\alpha}(\mathbf{x}))$ is given by:

$$\beta(\mathbf{x})=\left[\sqrt{r}\cos\frac{\theta}{2},\sqrt{r}\sin\frac{\theta}{2},\sqrt{r}\cos\frac{\theta}{2}\sin\theta,\sqrt{r}\sin\frac{\theta}{2}\sin\theta\right] \tag{11}$$

In Eq. (11) θ and r are local polar coordinates. After substituting the test and trial functions into Eq. (9) and employing nodal variations arbitrariness, the following discrete equations are obtained:

$$[\mathbf{K}]\{\mathbf{d}\}=\{\mathbf{f}\} \tag{12}$$

Here $\mathbf{d}$ is nodal unknowns' vector, $\mathbf{f}$ and $\mathbf{K}$ are externally applied force vector and global stiffness matrix respectively. By making use of the approximation functions for a crack, which are defined in Eq. (10), the element stiffness matrix $\mathbf{K}_{\mathbf{ij}}^{\mathbf{e}}$ and nodal vector force $\mathbf{f}^{\mathbf{e}}$ are obtained as follows:

$$\mathbf{K}_{\mathbf{ij}}^{\mathbf{e}}=\begin{bmatrix}\mathbf{K}_{ij}^{uu} & \mathbf{K}_{ij}^{ua} & \mathbf{K}_{ij}^{ub}\\ \mathbf{K}_{ij}^{au} & \mathbf{K}_{ij}^{aa} & \mathbf{K}_{ij}^{ab}\\ \mathbf{K}_{ij}^{bu} & \mathbf{K}_{ij}^{ba} & \mathbf{K}_{ij}^{bb}\end{bmatrix} \tag{13}$$

$$\mathbf{f}^{\mathbf{e}}=\left\{\mathbf{f}_{\mathbf{i}}^{\mathbf{u}} \quad \mathbf{f}_{\mathbf{i}}^{\mathbf{a}} \quad \mathbf{f}_{\mathbf{i}}^{\mathbf{b1}} \quad \mathbf{f}_{\mathbf{i}}^{\mathbf{b2}} \quad \mathbf{f}_{\mathbf{i}}^{\mathbf{b3}} \quad \mathbf{f}_{\mathbf{i}}^{\mathbf{b4}}\right\}^{T} \tag{14}$$

From Eq. (13) and Eq. (14), the following sub matrices are given:

$$\mathbf{K}_{\mathbf{ij}}^{\mathbf{rs}}=\int_{\mathbf{\Omega^e}}\left(\mathbf{B}_{\mathbf{i}}^{\mathbf{r}}\right)^{\mathbf{T}}\mathbf{D}\left(\mathbf{B}_{\mathbf{j}}^{\mathbf{s}}\right)d\Omega, \qquad (r,s=\mathbf{u},\mathbf{a},\mathbf{b}) \tag{15}$$

$$\mathbf{f}_{\mathbf{i}}^{\mathbf{u}}=\int_{\Gamma_{\mathbf{t}}}\Psi_j\bar{\mathbf{t}}\,d\Gamma+\int_{\mathbf{\Omega^e}}\Psi_j\mathbf{b}\,d\Omega \tag{16}$$

$$\mathbf{f}_{\mathbf{i}}^{a}=\int_{\Gamma\mathbf{t}}\Psi_j\left(H(\mathbf{x})-H(\mathbf{x}_{\mathbf{i}})\right)\bar{\mathbf{t}}\,d\Gamma+\int_{\mathbf{\Omega^e}}\Psi_j\left(H(\mathbf{x})-H(\mathbf{x}_{\mathbf{i}})\right)\mathbf{b}\,d\Omega \tag{17}$$

$$\mathbf{f}_{\mathbf{i}}^{b\alpha}=\int_{\Gamma\mathbf{t}}\Psi_j\left(\beta_{\alpha}(\mathbf{x})-\beta_{\alpha}(\mathbf{x}_{\mathbf{i}})\right)\bar{\mathbf{t}}\,d\Gamma+\int_{\mathbf{\Omega^e}}\Psi_j\left(\beta_{\alpha}(\mathbf{x})-\beta_{\alpha}(\mathbf{x}_{\mathbf{i}})\right)\mathbf{b}\,d\Omega \tag{18}$$

Ψ_j is standard FEM shape function, B_i^u, B_i^a, B_i^b and $\mathrm{B}_i^{b\alpha}$ are shape function derivatives matrices and given below:

$$\mathbf{B}_{\mathbf{i}}^{\mathbf{u}}=\begin{bmatrix}\Psi_{i,x} & 0\\ 0 & \Psi_{i,y}\\ \Psi_{i,y} & \Psi_{i,x}\end{bmatrix}_{3\times 8} \tag{19}$$

$$\mathbf{B}_{\mathbf{i}}^{\mathbf{a}}=\begin{bmatrix}\left(\Psi_i\left(H(\mathbf{x})-H(\mathbf{x}_{\mathbf{i}})\right)\right)_{,x} & 0\\ 0 & \left(\Psi_i\left(H(\mathbf{x})-H(\mathbf{x}_{\mathbf{i}})\right)\right)_{,y}\\ \left(\Psi_i\left(H(\mathbf{x})-H(\mathbf{x}_{\mathbf{i}})\right)\right)_{,y} & \left(\Psi_i\left(H(\mathbf{x})-H(\mathbf{x}_{\mathbf{i}})\right)\right)_{,x}\end{bmatrix} \tag{20}$$

$$\mathbf{B}_{\mathbf{i}}^{\mathbf{b}}=\left[\mathbf{B}_{\mathbf{i}}^{\mathbf{b1}} \quad \mathbf{B}_{\mathbf{i}}^{\mathbf{b2}} \quad \mathbf{B}_{\mathbf{i}}^{\mathbf{b3}} \quad \mathbf{B}_{\mathbf{i}}^{\mathbf{b4}}\right] \tag{21}$$

$$\mathbf{B}_{\mathbf{i}}^{\mathbf{b}\alpha}=\begin{bmatrix}\left(\Psi_i\left(\beta_{\alpha}(\mathbf{x})-\beta_{\alpha}(\mathbf{x}_{\mathbf{i}})\right)\right)_{,x} & 0\\ 0 & \left(\Psi_i\left(\beta_{\alpha}(\mathbf{x})-\beta_{\alpha}(\mathbf{x}_{\mathbf{i}})\right)\right)_{,y}\\ \left(\Psi_i\left(\beta_{\alpha}(\mathbf{x})-\beta_{\alpha}(\mathbf{x}_{\mathbf{i}})\right)\right)_{,y} & \left(\Psi_i\left(\beta_{\alpha}(\mathbf{x})-\beta_{\alpha}(\mathbf{x}_{\mathbf{i}})\right)\right)_{,x}\end{bmatrix} \tag{22}$$

$\alpha=1,2,3,4$

The basic and fundamental conception of LEFM is applicable if and only if the plastic deformation at the crack tip is small. According to (Anderson, 2017) the stress state at the neighborhood of the crack front is given as

$$\sigma_{ij} = \frac{1}{\sqrt{2\pi r}}\left[K_I f_{ij}^{I}(\theta) + K_{II} f_{ij}^{II}(\theta) + K_{III} f_{ij}^{III}(\theta)\right] \quad (23)$$

where K_I, K_{II} and K_{III} are SIFs for mode I (opening), II (Shear) and III (out-of-plane shear) respectively. $f_{ij}(\theta)$ denotes dimensionless trigonometric function of θ. Stress and displacement field equations in the vicinity of the tip for the three fracture modes are summarized in Table 1 and Table 2 respectively (Anderson, 2017) .

Table 1. Crack Tip Stress Fields for Modes I and II (Anderson, 2017)

	Mode I	Mode II
σ_{xx}	$\frac{K_I}{\sqrt{2\pi r}}\cos\frac{\theta}{2}\left(1-\sin\frac{\theta}{2}\sin\frac{3\theta}{2}\right)$	$-\frac{K_{II}}{\sqrt{2\pi r}}\sin\frac{\theta}{2}\left(2+\cos\frac{\theta}{2}\cos\frac{3\theta}{2}\right)$
σ_{yy}	$\frac{K_I}{\sqrt{2\pi r}}\cos\frac{\theta}{2}\left(1+\sin\frac{\theta}{2}\sin\frac{3\theta}{2}\right)$	$\frac{K_{II}}{\sqrt{2\pi r}}\sin\frac{\theta}{2}\cos\frac{\theta}{2}\cos\frac{3\theta}{2}$
σ_{xy}	$\frac{K_I}{\sqrt{2\pi r}}\sin\frac{\theta}{2}\cos\frac{\theta}{2}\cos\frac{3\theta}{2}$	$\frac{K_{II}}{\sqrt{2\pi r}}\cos\frac{\theta}{2}\left(1-\sin\frac{\theta}{2}\sin\frac{3\theta}{2}\right)$
σ_{zz}	$\nu(\sigma_{xx}+\sigma_{yy})$; $\tau_{xz}=\tau_{yz}=0$	$\nu(\sigma_{xx}+\sigma_{yy})$; $\tau_{xz}=\tau_{yz}=0$

Table 2. Displacement Fields in front of Crack Tip for Modes I and II (Anderson, 2017)

	Mode I	Mode II
u_x	$\frac{K_I}{2\mu}\sqrt{\frac{r}{2\pi}}\cos\frac{\theta}{2}\left(\kappa-1+2\sin^2\frac{\theta}{2}\right)$	$\frac{K_{II}}{2\mu}\sqrt{\frac{r}{2\pi}}\sin\frac{\theta}{2}\left(\kappa+1+2\cos^2\frac{\theta}{2}\right)$
u_y	$\frac{K_I}{2\mu}\sqrt{\frac{r}{2\pi}}\sin\frac{\theta}{2}\left(\kappa+1-2\cos^2\frac{\theta}{2}\right)$	$\frac{K_{II}}{2\mu}\sqrt{\frac{r}{2\pi}}\cos\frac{\theta}{2}\left(\kappa-1-2\sin^2\frac{\theta}{2}\right)$

The symbols in the Tables are as follows: ν denotes Poisson's ratio, $\mathbf{E}$ signifies modulus of elasticity, κ denotes Kolosov constant and μ denotes the shear modulus. κ and μ can be written as:

$$\kappa=(3-4\nu) \qquad \text{Plane strain} \quad (24)$$

$$\kappa=\frac{(3-\nu)}{(1+\nu)} \qquad \text{Plane stress} \quad (25)$$

$$\mu=\frac{\mathbf{E}}{2\,(1+\nu)} \quad (26)$$

4. Results and discussion

The first example considered straight edge configuration shown in Figure 1by comparing XFEM results with the closed form solution as proposed in (Tada et al., 2000).

$$K_I = f\sigma_o\sqrt{\pi a}$$
$$f = 1.122 - 0.231(a/L) + 10.55(a/L)^2 - 21.72(a/L)^3 + 30.382(a/L)^4 \tag{27}$$

In this example the mixed mode SIFs (K_I and K_{II}) are computed using domain based interaction integral (Moran and Shih, 1987; Sukumar et al., 2000). Firstly, normalized SIF (K_I) with respect to a/L ratio for horizontal edge crack (β=0 and d/D=0) was estimated and the result compared with that of the closed form solution from reference (Tada et al., 2000). From Fig. 4, the theoretical results are in agreement with the present result.

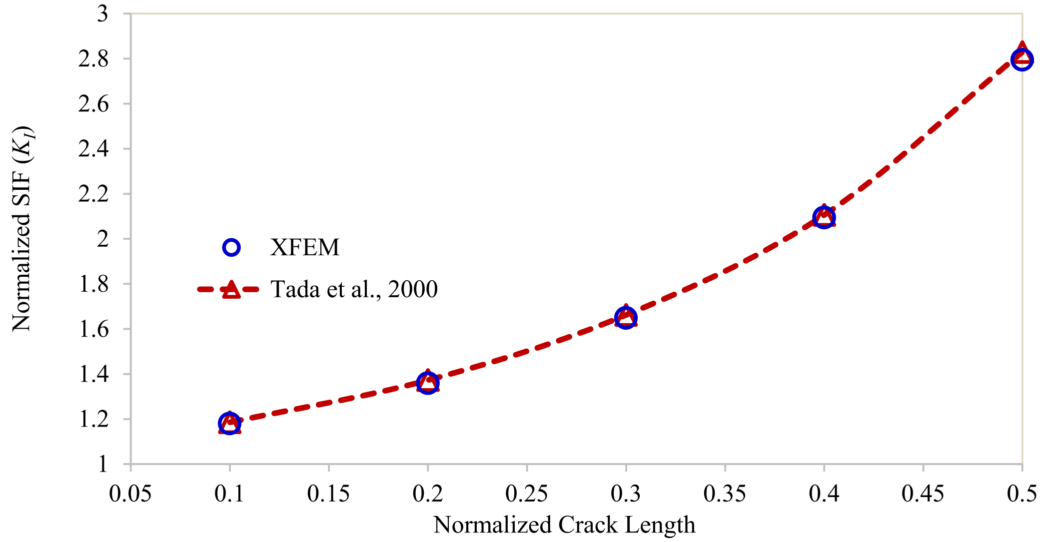

Fig. 4. Comparative study on the variation of Normalized SIF with normalized crack length (Tada et al., 2000)

Fig. 5 and Fig. 6 present the convergence and error estimation for mode-I SIF for different number of nodes respectively. From Fig. 5, the estimated value of K_I converges to the closed form solution as the number of nodes increases. Similarly the percentage error gets reduced and closer to zero as number of nodes increases, as depicted in Fig. 6. Therefore the number of nodes considered in this study is 50 by 100.

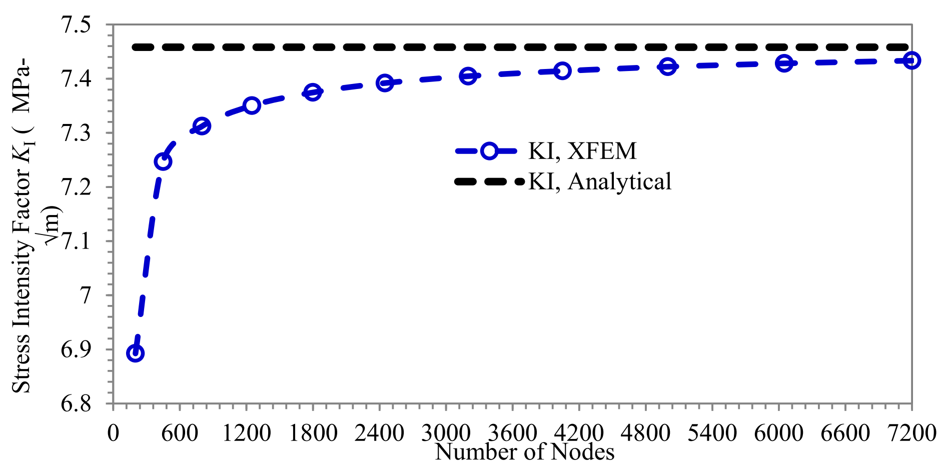

Fig. 5. Comparative study of K_I values between XFEM and closed form solution for different number of nodes.

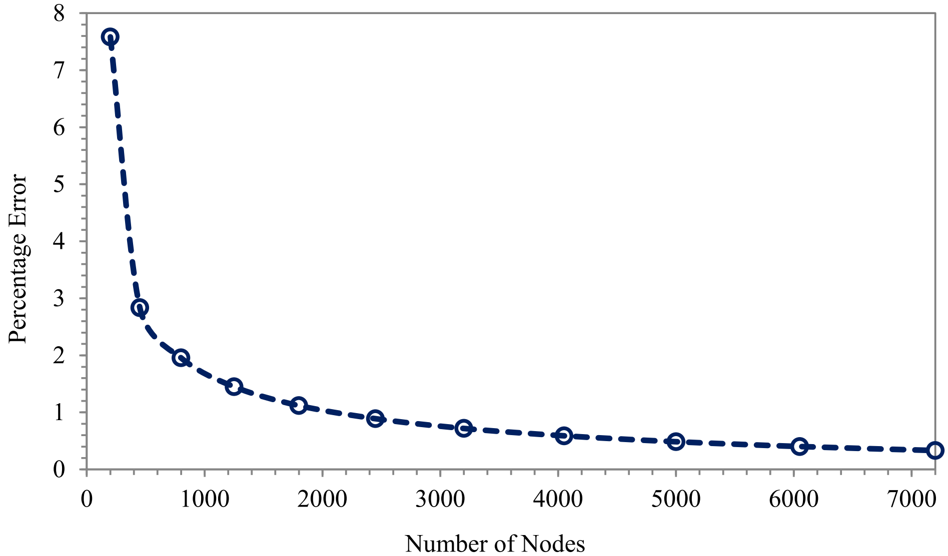

Fig. 6. Percentage error in relation to number of nodes

To demonstrate the effectiveness of XFEM, a comparative study between applied stresses (σ_o) and SIF (K_I) has been conducted. SIF is plotted against the applied stress (σ_o) and it is observed that results from XFEM show good agreement with (Tada et al., 2000) as depicted in Fig. 7. The stress contours σ_{xx}, σ_{xy} and σ_{yy} are also shown in Fig. 8 (a), Fig. 8 (b) and Fig. 8 (c) and witnessed that the stress values at the crack tip are maximum as expected.

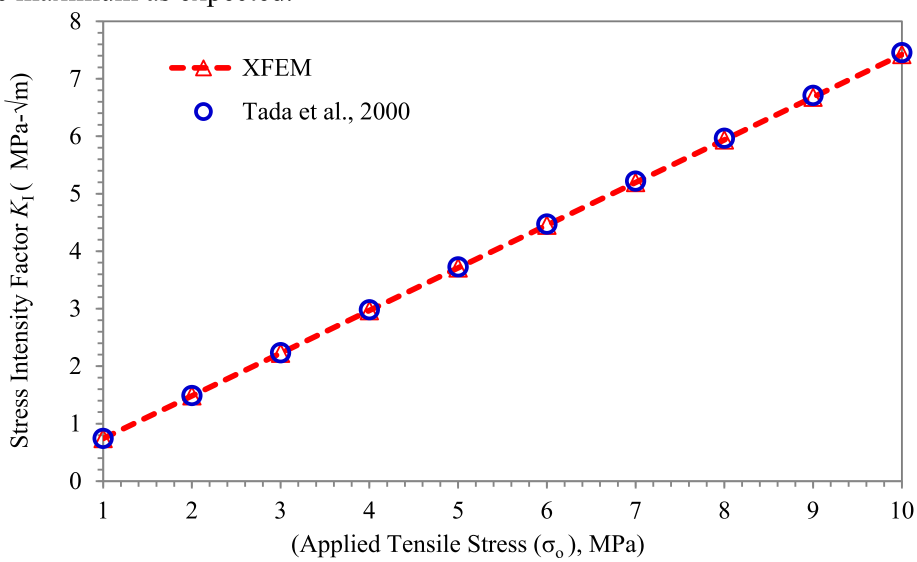

Fig. 7. Comparative analysis of K_I values with closed form solutions for different values of applied tensile stresses

Fig. 9 and Fig. 10 demonstrate how the normalized crack size (*a/L*) and inclination angle of the crack affect mode I SIFs and mode II SIFs respectively. In this particular example d/*D* ratio is considered to be 0. As observed from Fig. 9 for each and discrete normalized crack size (*a/L*) mode I SIF decreases and approaches to zero as the crack inclination angle (β) increases. In other words for each and every inclination angle β as crack size increases so does the mode I SIF. It is also noticed from Fig. 9 that the effect of crack inclination angle on the level of increase of the normalized mode I SIF is more dominant at smaller crack angles. For crack inclination angles greater that 60º it is observed that crack size has no significant effect on the normalized SIF (K_I), this is possibly due to the decrease in the normal force contribution on the crack surface. XFEM result has been compared with results from literature (Fayed, 2017) and good agreements have been observed as in Fig. 9.

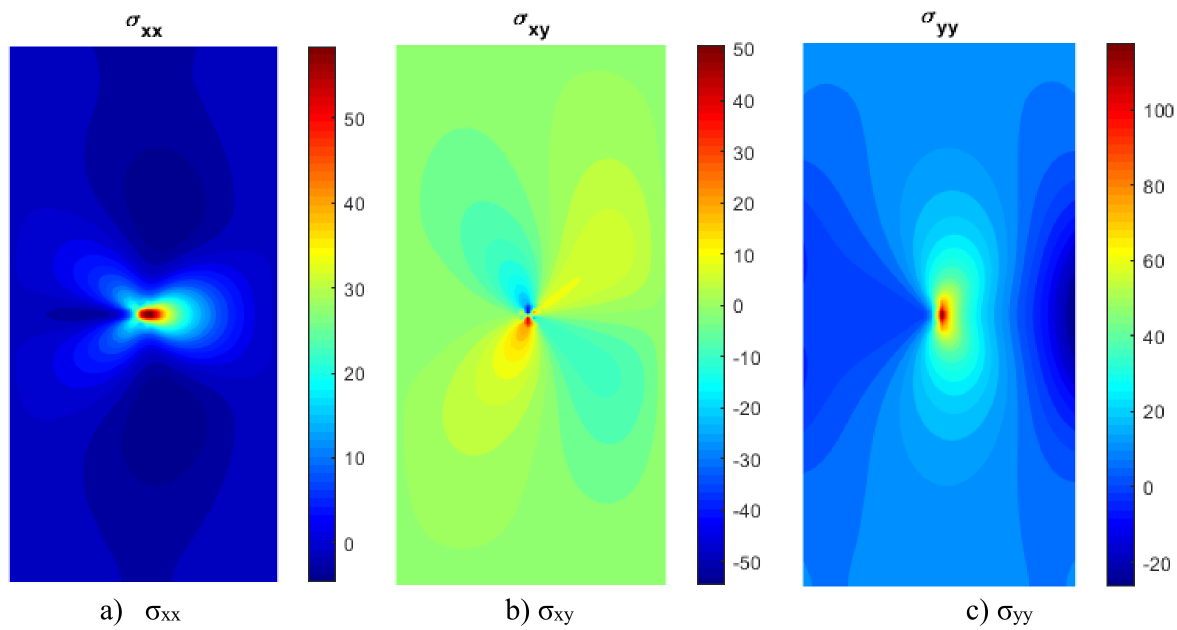

Fig. 8. Stress contour for an edge crack

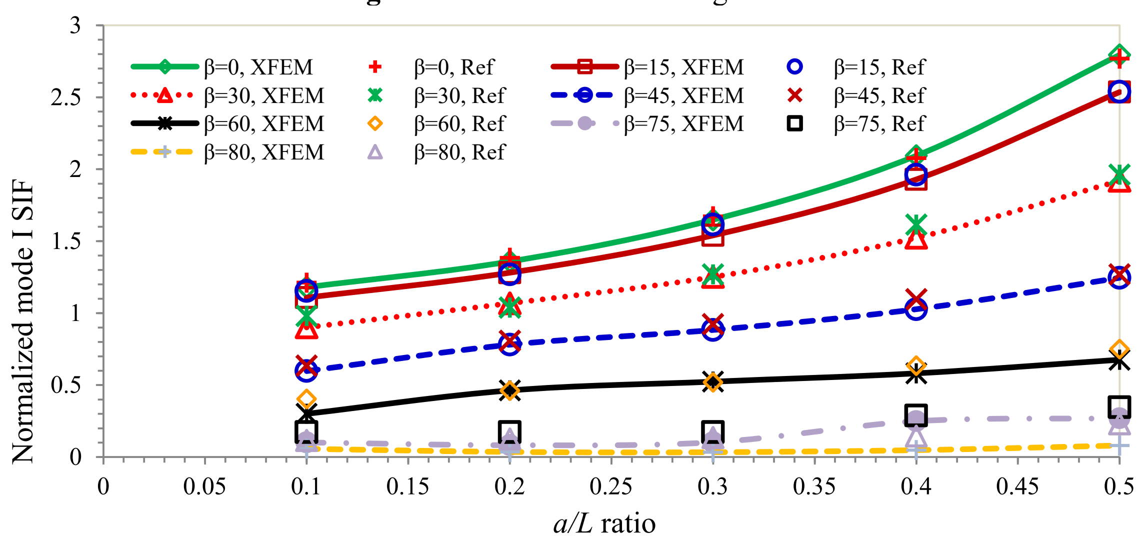

Fig. 9. Effect of crack inclination angle on normalized mode I SIF.

Fig. 10 shows a comparative study among the normalized mode II SIF (K_{II}) and crack inclination angle β. It is clear from Fig. 10 that the values of the normalized mode II SIF (K_{II}) escalates from its minimum value zero where β = 0 to its maximum value and then decline towards zero when β approaches 90°. The normalized mode II SIF (K_{II}) attains its maximum value when β is between 30° and 50°. Here again, XFEM result has been compared with results from literature (Fayed, 2017) and good agreements has been observed as in Fig. 10. Furthermore Fig. 11 illustrates a comparative study between mode I SIF (K_I) and crack inclination angle β. In this example *d/D* ratio was considered to be 0. It is clearly observed from Fig. 11 that the values of the normalized mode I SIF (K_I) keeps declining from its maximum value where β = 0 to its minimum value close to zero when β approaches 80°. Here also a close agreement between XFEM result and results from literature was noticed (Fayed, 2017). Similarly Figs. 12 (a), (b) and (c) show stress contours σ_{xx}, σ_{xy} and σ_{yy} in the case of inclined crack respectively.

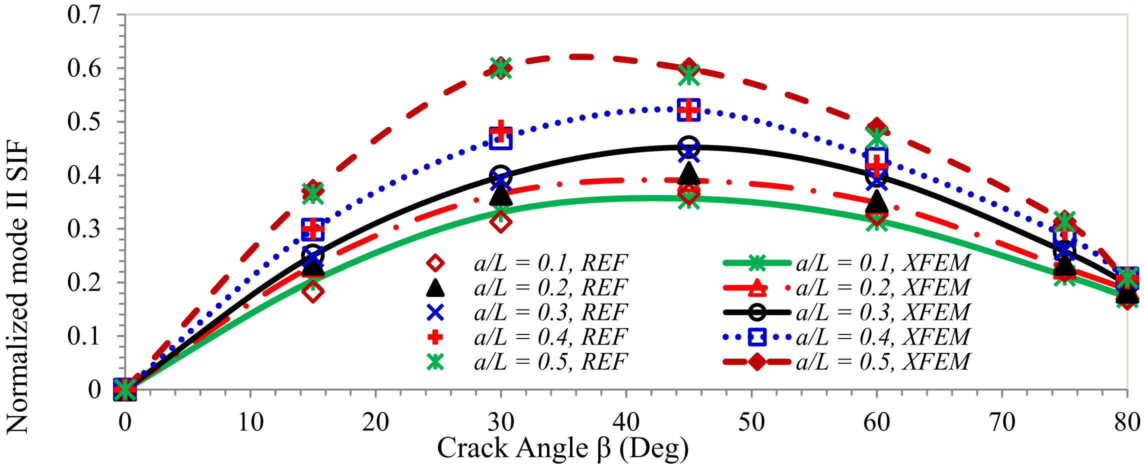

Fig. 10. The effect of crack inclination angle on normalized SIF (K_{II}).

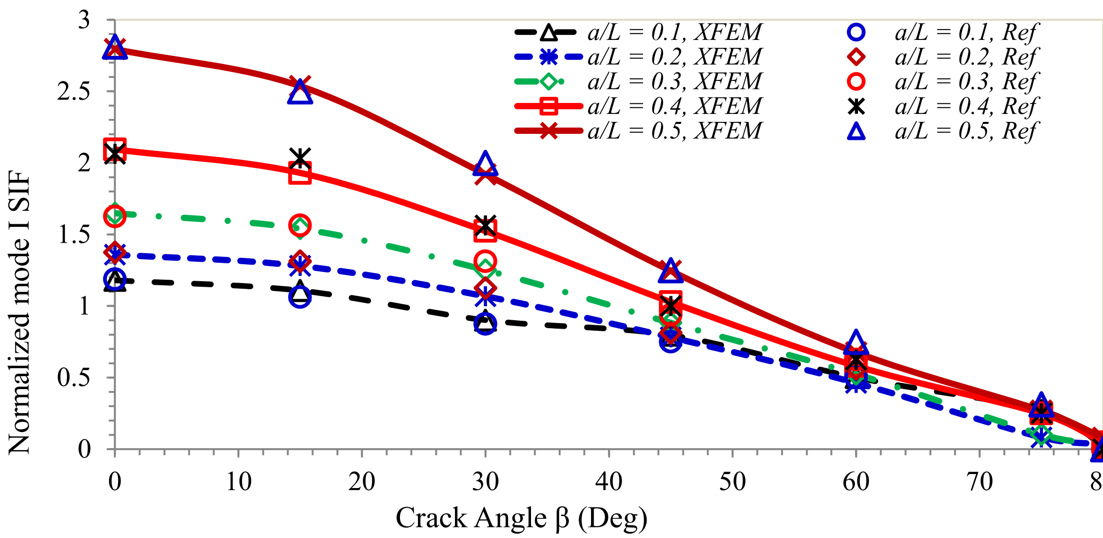

Fig. 11. Effect of crack length to width ratio (a/L) on normalized SIF (K_I)

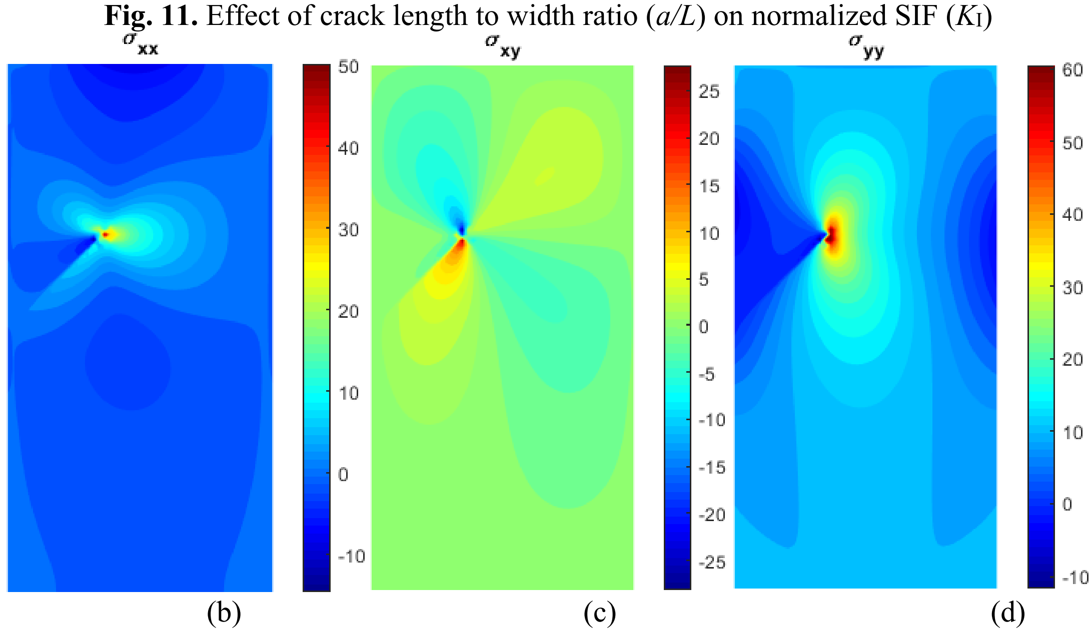

Fig. 12. Stress contour for an edge crack.

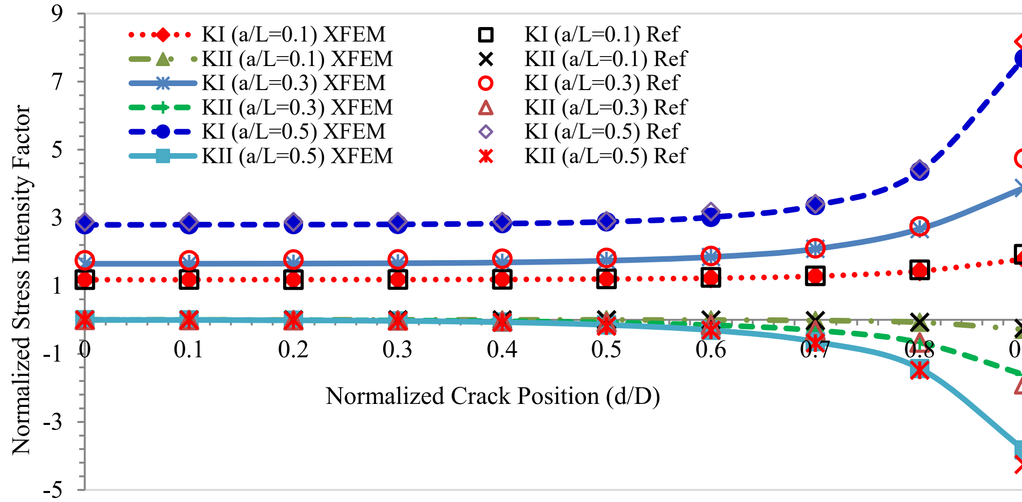

(a)

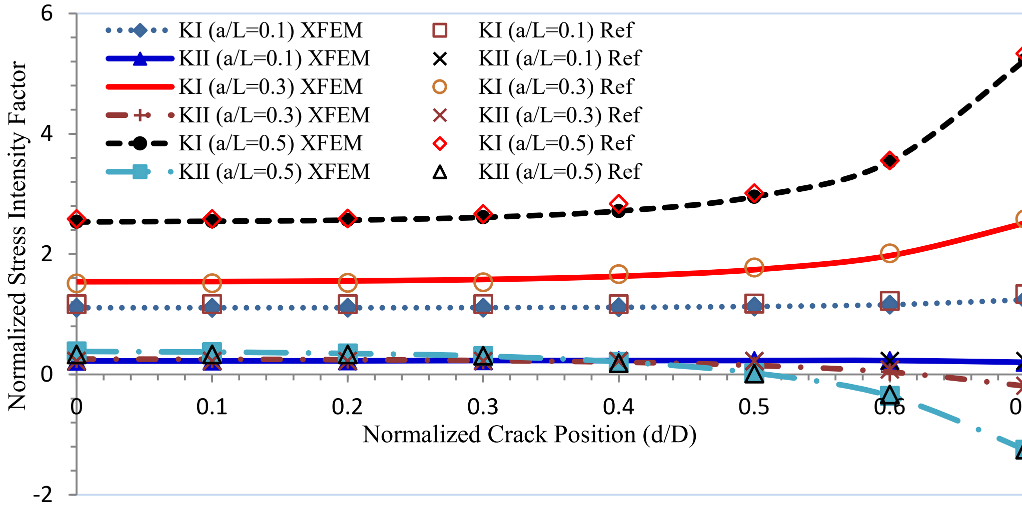

(b)

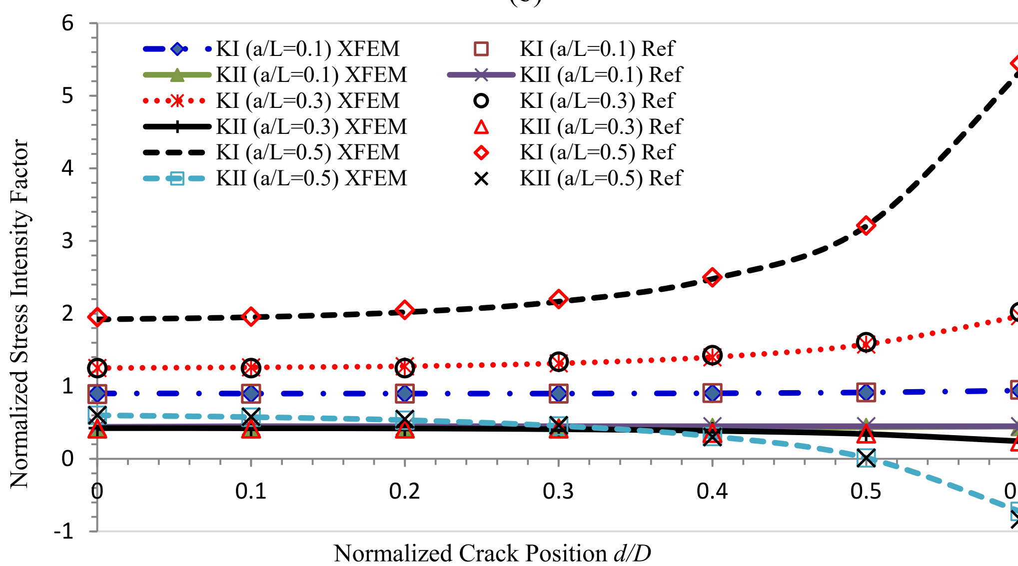

(c)

Fig. 13. The effect of crack position on K_{I} and K_{II}, (a) β = 0, (b) β = 15 and (c) β = 30.

The other parameter we considered in this study was the effect of crack position on the SIFs (I and II) as presented in Fig. 13 for different crack inclination angles and crack size. The results obtained from XFEM have been compared with results from the reference (Fayed, 2017). As it is illustrated in Fig. 13 (a) the change in crack positioning in the vertical axis results in an increase in K_I. It is also observed that the rate of increase of K_I is not noticeable for some *d/D* ratio until a certain *d/D* ratio for each crack size and inclination angle beyond which it increases faster. This rate of increase in SIF is a function of crack inclination angle and size as it is clearly observed from Fig. 13. The increase in K_I and K_{II} between 0 and 0.6 *d/D* ratio when *a/L*=0.1 is not noticeable whereas at a/L ratio of 0.8 and above it attains its maximum value. But in case of *a/L* ratio of 0.3 and 0.5 the increase in SIF (K_I and K_{II}) become more noticeable at higher angles.

5. Conclusions

Extended Finite Element Method (X-FEM) was implemented in this study for estimation of crack propagation in a material. The approach employed in this study is extremely vital due to the fact that it does not require multiple remeshing which is quite mandatory in the case of FEM when the cracks start moving. In this article, tensile load has been applied on the top face of a slanted edge cracked plate remotely to compute the mixed mode SIFs (K_I/K_{II}). The effects of different parameters like cracking angle and its location, crack position along the vertical axis and crack length to width ratio (*a/L*) have been considered in the determination of SIFs. By taking into account the aforementioned parameters, the mixed mode SIFs (K_I/K_{II}) has been determined. The results obtained from XFEM remarkably agreed with those from literature and hence justified the prominent performance of the method to compute SIF for mode I and mode II.

References

Aliha, M.R., Bahmani, A., & Akhondi, S. (2016). Mixed mode fracture toughness testing of PMMA with different three-point bend type specimens. *European Journal of Mechanics-A/Solids, 58*, 148-162.

Ameri, B., Taheri-Behrooz, F., & Aliha, M. R. M. (2021). Evaluation of the Geometrical Discontinuity effect on Mixed-Mode I/II Fracture Load of FDM 3D-Printed Parts. *Theoretical and Applied Fracture Mechanics, 113*, 102953.

Anderson, T. L. (2017). *Fracture mechanics: fundamentals and applications*. CRC press.

Barsoum, R. S. (1974). Application of Quadratic Isoparametric Finite Elements in Linear Fracture Mechanics. *International Journal of Fracture, 10*(4), 603-605.

Belytschko, T., & Black, T. (1999). Elastic crack growth in finite elements with minimal remeshing. *International Journal for Numerical Methods in Engineering, 45*, 601–620.

Belytschko, T., Gu, L., & Lu, Y. Y. (1994). Fracture and crack growth by element free Galerkin methods. *Modelling and Simulation in Materials Science and Engineering, 2*(3A), 519.

Belytschko, T., Liu, W. K., Moran, B., & Elkhodary, K. I. (2014). *Nonlinear Finite Elements for Continua and Structures*. 2nd ed . Chichester: Wiley.

Belytschko, T., Lu, Y. Y., & Gu, L. (1994). Elementfree Galerkin methods. *International Journal for Numerical Methods in Engineering, 37*(2), 229-256.

Bhadauria, S. S., Pathak, K. K., & Hora, M. S. (2010). Finite element modeling of crack initiation angle under mixed mode (I/II) fracture. *Journal of Solid Mechanics, 2*, 231-247.

Bouhala, L., Shao, Q., Koutsawa, Y., Younes, A., Núñez, P., Makradi, A., et al. (2013). An XFEM crack-tip enrichment for a crack terminating at a bi-material interface. *Engngineering Fracture Mechanics, 102*, 51–64.

Ching, H. K., & Yen, S. C. (2005,). Meshless local petrov-Galerkin analysis for 2D functionally graded elastic solids under mechanical and thermal loads. *Composites Part B: Engineering, 36*(3), 223–40.

El Fakkoussi, S., Moustabchir, H., Elkhalfi, A., & Pruncu, C. I. (2019). Computation of the stress intensity factor KI for external longitudinal semi-elliptic cracks in the pipelines by FEM and XFEM methods. *International Journal of Interaction Design Manufacturing, 13*, 545–555.

Fayed, A. S. (2017). Numerical analysis of mixed mode I/II stress intensity factors of edge slant cracked plates. *Engineering Solid Mechanics, 5*(1), 61-70.

Gonzalez, M., Teixeira, P., Wrobel, L. C., & Martinez, M. (2015). A new Displacement-based Approach to Calculate Stress Intensity Factors With the Boundary Element Method. *Latin American Journal of Solids and Structures, 12*(9), 1677-1697.

Griffith, A. (1920). The Phenomena of Rupture and Flow in Solids. *Philosophical Transactions, Series A, 221*, 163-198.

Gu, Y., Wang, W., Zhang, L. C., & Feng, X. Q. (2011). An enriched radial point interpolation method (e-RPIM) for analysis of crack tip fields. *Engineering Fracture Mechanics, 78*(1), 175–90.

Han, Q., Wang, Y., Yin, Y., & Wang, D. (2015). Determination of stress intensity factor for mode I fatigue crack based on finite element analysis. *Engineering Fracture Mechanics , 138*, 118-126 .

Hedayati, E., & Vahedi, M. (2014). Using Extended Finite Element Method for Computation of the Stress Intensity Factor, Crack Growth Simulation and Predicting Fatigue Crack Growth in a Slant-Cracked Plate of 6061-T651 Aluminum. *World Journal of Mechanics, 4*, 24-30.

Hellen, T. K. (1975). On the Method of Virtual Crack Extension. *International Journal for Numerical Methods in Engineering, 9*(1), 187-207.

Henshell, R. D., & Shaw, K. G. (1975). Crack Tip Finite Elements Are Unnecessary. *International Journal for Numerical Methods in Engineering, 9*(3), 495-507.

Irwin, G. (1957). Analysis of Stresses and Strains Near the End of a Crack Traversing a Plate. *Journal of Applied Mechanics, 24*, 361-364.

Laftah, R. M. (2016). Study of Stress Intensity Factor in Corrugated Plate Using Extended Finite Element Method (XFEM). *Engineering & Technical Journal, Part (A), 34*(15), 2982-2992.

Lee, S. H., Kim, K. H., & Yoon, Y. C. (2016). Particle difference method for dynamic crack propagation. *International Journal of Impact Engineering, 87*, 132–145.

Leung, A. Y., Zhou, Z., & Xu, X. (2014)). Determination of stress intensity factors by the finite element discretized symplectic method. *International Journal of Solids and Structures, 51*(5), 1115-1122 .

Lins, R., Ferreira, M., & Proença, S. e. (2015). An a-posteriori error estimator for linear elastic fracture mechanics using the stable generalized/extended finite element method. *Computer Mechanics, 56*, 947-965.

Liu, W. K., Jun, S., & Zhang, Y. F. (1995). Reproducing kernel particle methods. *International Journal of Numerical Methods Fluids, 20*(8–9), 1081–11066.

Lu, Y. Y., Belytschko, T., & Gu, L. (1994). A new implementation of the element free Galerkin method. *Computational Methods in Applied Mechanical Engineering, 113*(3-4), 397–414.

Menk, A., & Bordas, S. P. (2011). Crack growth calculations in solder joints based on microstructural phenomena with x-fem. *Computational Materials Science, 50*(3), 1145–1156.

Mirmohammad, S. H., Safarabadi, M., Karimpour, M., Aliha, M. R. M., & Berto, F. (2018). Study of composite fiber reinforcement of cracked thin-walled pressure vessels utilizing multi-scaling technique based on extended finite element method. *Strength of Materials, 50*(6), 925-936.

Moes, N., Dolbow, J., & Belytschko, T. (1999). A finite element method for crack growth without remeshing. *International Journal for Numerical Methods in Engineering, 46*, 131-150.

Moran, B., & Shih, C. F. (1987). Crack tip and associated domain integrals from momentum and energy balance. *Engineering Fracture Mechanics, 27*(6), 615-642.

Murakami, Y., & Keer, L. M. (1993). *Stress Intensity Factors Handbook* (Vol. 3).

Ortiz, J. E., & Cisilino, A. P. (2006). Boundary element method for J-integral and stress intensity factor computations in three-dimensional interface cracks. *International Journal of Fracture, 133*(3), 197-222.

Pais, M. (2011). Variable Amplitude Fatigue Analysis Using Surrogate Models and Exact XFEM Reanalysis. University of Florida.

Paris, P., & Erdogan, F. (1963). A critical analysis of crack propagation laws. *Journal of Basic Engineering Transaction of ASME, 85*, 528-534.

Parks, D. M. (1974). A Stiffness Derivative Finite Element Technique for Determination of Crack Tip Stress Intensity Factors. *International Journal of Fracture, 10*, 487-502.

Pommier, S., Gravouil, A., Combescure, A., & Moës, N. (2011). Extended finite element method for crack propagation. London, UK: ISTE.
Portela, A., Aliabadi, M. H., & Rooke, D. P. (1992). The dual boundary element method: effective implementation for crack problems. *International Journal for Numerical Methods in Engineering, 33*(6), 1269-1287.
Rabczuk, T., & Belytschko, T. (2004). Cracking particles: a simplified meshfree method for arbitrary evolving cracks. *International Journal for Numerical Methods in Engineering, 61*(13), 2316-2343.
Rice, R. J. (1968). A Path Independent Integral and the Approximate Analysis of Strain Concentrations by Notches and Cracks. *Journal of Applied Mechanics, 35*, 379-386.
Rybicki, E. F., & Kanninen, M. F. (1977). A Finite Element Calculation of Stress Intensity Factors by a Modified Crack Closure Integral. *Engineering Fracture Mechanics, 9*(4), 931-938.
Shih, C. F., De Lorenzi, H. G., & German, M. D. (1976). Crack Extension Modeling with Singular Quadratic Isoparametric Element. *International Journal of Fracture, 12*(4), 647-651.
Singh, I. V., Mishra, B. K., Bhattacharya, S., & Patil, R. U. (2012). The numerical simulation of fatigue crack growth using extended finite element method. *International Journal of Fatigue, 36*(1), 109-119.
Stern, M., Becker, E. B., & Dunham, R. S. (1976). A contour integral computation of mixed-mode stress intensity factors. *International Journal of Fracture, 12,* 359-68.
Sukumar, N., Chopp, D. L., Moës, N., & Belytschko, T. (2001). Modeling holes and inclusions by level sets in the extended finite element method. *Computer Methods in Applied Mechanical Engineering, 190*(46-47), 6183–6200.
Sukumar, N., Moes, N., Moran, B., & Belytschko, T. (2000). Extended Finite element method for three-dimensional crack modelling. *International Journal of Numerical Methods in Engineering, 48*, 1549 -1570.
Szabo, B. A., & Babuška, I. (1988). Computation of the Amplitude of Stress Singular Terms for Cracks and Reentrant Corners. In Fracture mechanics: nineteenth symposium (pp. 101-124). West Conshohocken: ASTM International.
Tada, H., Paris, P., & Irwin, G. (2000). *The Stress Analysis of Cracks Handbook.* 3rd ed., New York.